EPJ Web of Conferences **272**, 01012 (2022) https://doi.org/10.1051/epjconf/202227201012
QENS/WINS 2022

Revisiting the modeling of quasielastic neutron scattering from bulk water

Martin H. Petersen[1,*], *Mark T. F.* Telling[2,**], *Gerald* Kneller[3,4,***] and *Heloisa N.* Bordallo[1,5,****]

[1]Niels Bohr Institute, University of Copenhagen, Universitetsparken 5, 2100 Copenhagen, Denmark
[2]STFC ISIS Facility Rutherford Appleton Laboratory, Harwell Campus, Oxfordshire, OX11 0QX, UK
[3]Centre de Biophysique Moléculaire, CNRS and Université d'Orléans, Rue Charles Sadron, 45071 Orléans, France
[4]Synchrotron Soleil, L'Orme de Merisiers, 91192 Gif-sur-Yvette, France
[5]European Spallation Source ERIC Box 176, SE-221 00, Lund, Sweden

Abstract. Quasi-elastic neutron scattering (QENS) from bulk-water at 300 K, measured on the IRIS backscattering neutron spectrometer (ISIS, UK), is interpreted using the jump diffusion model (JDM), a "minimalistic" multi-timescale relaxation model (MRM) and molecular dynamics simulations (MD). In the case of MRM data analysis is performed in the time domain, where the relaxation of the intermediate scattering function is described by a stretched Mittag-Leffler function, $E_\alpha(-(|t|/\tau)^\alpha)$. This function displays an asymptotic power law decay and contains the exponential relaxation function as a special case ($\alpha = 1$). To further compare the two approaches, MD simulations of bulk water were performed using the SPCE force field and the resulting MD trajectories analysed using the nMoldyn software. We show that both JDM and MRM accurately describe the diffusion of bulk water observed by QENS at all length scales, and confirm that MD simulations do not fully describe the quantum effects of jump diffusion.

1 Introduction

Quasi-elastic neutron scattering (QENS) is a powerful spectroscopic technique used to explore diffusive motions of atoms on length scale between 1 Å and 100 Å and times scales between 10^{-9}s and 10^{-13}s. Because of the dominant incoherent scattering response from hydrogen atoms, QENS studies explore, in particular, the diffusive motions of individual hydrogen atoms and are thus ideal to study water dynamics. Considering the study of bulk-water, the QENS spectra cannot be completely described by a small-step diffusion model for free diffusion. This happens because the diffusion in liquids takes place in discrete diffusive jumps [1] and a corresponding model for simple liquids was formulated by Chudley, using both Schofield's semiclassical approximation [2] and Van Hove's formalism of correlation functions [3]. Following these ideas, Teixeira *et al.* [4] extended the model for water, including vibrational and rotational degrees of freedom. As with any "spatial motion model" [5], the resulting intermediate scattering function is composed of several Lorentzians, related to different motion types. The ability to rationalize QENS data in terms of a relatively small number of parameters makes this approach widely adopted in QENS data analysis for a variety of other systems [6, 7, 8, 9, 10, 11]. Although successful, the method described in [4] requires prior information of the system, since it is essential to attribute each Lorentzians needed to represent the measured dynamics to a specific motion. A good example here is the confined water in clay minerals, where different populations of water molecules coexist [7, 10]. To avoid such *a priori* assumptions, alternative approaches for interpreting QENS data are urgently needed. Having that in mind, a "minimal model approach", where the multi-scale relaxation of the water molecules can be described without any prior information [12], has been recently proposed and successfully used to analyse the dynamics of confined water molecules in proteins and clay minerals [13, 14, 15]. This said analysis shows that the new method can capture the full dynamics of the confined water with the benefit that it rationalizes extensive sets of QENS data in terms of a minimal number of parameters. Here we apply both methods to analyse bulk water, H_2O, at $300K$.

To further understand the differences and similarities between the two approaches, a complementary technique is needed. Molecular dynamics (MD) simulation is the method of choice since it provides detailed information about the dynamics of molecules and atoms of complex systems within the length and time scale probed by QENS. Considering the system of bulk-water, we can then compare the motion of water molecules seen by MD trajectories with those probed experimentally and, as a "side effect", verify the simulations [16]. For this purpose, MD simulations have been performed for bulk-water at $300K$ using the LAMMPS Molecular Dynamics Simulator with the Velocity-Verlet algorithm as its numerical solver. To directly compare the measured QENS spectra to the MD results, the conversion of the trajectories and velocities to either $S(Q,\omega)$ or its Fourier transformed

*e-mail: martinhp27@gmail.com
**e-mail: mark.telling@stfc.ac.uk
***e-mail: gerald.kneller@cnrs.fr
****e-mail: bordallo@nbi.ku.dk

$F(Q,t)$ was carried out using the program package nMoldyn [17, 18, 19, 20].

2 Neutron scattering functions

2.1 Dynamic structure factor

In a standard QENS experiment from hydrogen rich systems one measures the dynamic structure factor [4, 6],

$$S(\mathbf{Q},\omega) = \frac{1}{2\pi}\int_{-\infty}^{+\infty} dt\, e^{-i\omega t} F(\mathbf{Q},t), \tag{1}$$

which is the time Fourier transform of the intermediate scattering function containing within it information about the structural dynamics of the system under consideration; $|\mathbf{Q}| = Q$ being the magnitude of the scattering vector and $\hbar\omega$ the energy transferred between the neutron and the nucleus.

Defining $\hat{\mathbf{R}}_j(t)$ as the time-dependent position operator of scattering atom j, we have

$$F(\mathbf{Q},t) \approx \frac{1}{N}\sum_{j=1}^{N}\left\langle e^{-i\mathbf{Q}\cdot\hat{\mathbf{R}}_j(0)} e^{i\mathbf{Q}\cdot\hat{\mathbf{R}}_j(t)}\right\rangle, \tag{2}$$

where $\langle\ldots\rangle$ denotes a quantum ensemble average summed over all N hydrogen atoms. We note in this context that $\hbar\omega$ is the energy transfer from the neutron to the sample.

The intermediate scattering function and the dynamic structure factor fulfill the symmetry relations

$$F(\mathbf{Q},-t) = F(-\mathbf{Q},t+i\beta\hbar), \tag{3}$$

$$S(\mathbf{Q},\omega) = e^{\beta\hbar\omega} S(-\mathbf{Q},-\omega), \tag{4}$$

where $\beta = 1/k_B T$ is the inverse Boltzmann temperature. Equation (4) is the well-known detailed-balance relation.

2.2 Generic form of $F(\mathbf{Q},t)$

For the further considerations we write the intermediate scattering function in the generic form [12, 13, 14],

$$F(\mathbf{Q},t) = (1 - EIS\,F(\mathbf{Q}))\phi(\mathbf{Q},t) + EIS\,F(\mathbf{Q}) \tag{5}$$

where $(1 - EIS\,F(\mathbf{Q}))$ and $EIS\,F(\mathbf{Q})$ are, respectively, the quasi-elastic and elastic amplitudes and $\phi(\mathbf{Q},t)$ is an atom-averaged normalized self-correlation function describing the relaxation dynamics of the hydrogen atoms,

$$\phi(\mathbf{Q},t) = \frac{1}{N_H}\frac{\sum_\alpha \left\langle \delta\bar{\rho}_\alpha^\dagger(\mathbf{Q},0)\delta\bar{\rho}_\alpha(\mathbf{Q},t)\right\rangle}{\sum_\alpha \left\langle \delta\bar{\rho}_\alpha^\dagger(\mathbf{Q},0)\delta\bar{\rho}_\alpha(\mathbf{Q},0)\right\rangle}. \tag{6}$$

Here the sum $\sum_\alpha$ runs over all hydrogen atoms, where N_H is their total number and $\delta\bar{\rho}_\alpha(Q,t) = \bar{\rho}_\alpha(Q,t) - \langle\bar{\rho}_\alpha(Q)\rangle$ is the deviation of the spatially Fourier-transformed single particle density of atom α, $\bar{\rho}_\alpha(\mathbf{Q},t) = e^{i\mathbf{Q}\cdot\hat{\mathbf{R}}_j(t)}$, with respect to its mean value. By construction, $\phi(\mathbf{Q},t)$ has the same symmetry properties as the intermediate scattering function and must satisfy $\phi(\mathbf{Q},0) = 1$ and $\lim_{t\to\infty}\phi(\mathbf{Q},t) = 0$.

Since we consider here scattering from an isotropic sample, $S(\mathbf{Q},\omega) = S(Q,\omega)$ and $F(\mathbf{Q},t) = F(Q,t)$, and $Q \equiv |\mathbf{Q}|$.

2.3 Semiclassical approximation

We now introduce the symmetrized and normalized relaxation function [14],

$$\phi^{(+)}(Q,t) = \frac{\phi(Q,t+i\beta\hbar/2)}{\phi(Q,i\beta\hbar/2)}, \tag{7}$$

which is real and symmetric in time, and the corresponding intermediate scattering function,

$$F^{(+)}(Q,t) = (1 - EIS\,F(Q))\phi^{(+)}(Q,t) + EIS\,F(Q). \tag{8}$$

The choice of using $\phi^{(+)}(Q,t)$ instead of $\phi(Q,t)$ is motivated by Schofield's semi-classical correction [2], which consists of relating the shifted relaxation function with its classical counterpart [14],

$$\phi^{(+)}(Q,t) \approx \phi^{(cl)}(Q,t), \tag{9}$$

and is valid up to the first order in $\hbar$, giving some justification for analyzing QENS data with classical diffusion models [2, 13].

3 QENS models

3.1 Jump diffusion model (JDM)

To obtain the half-width at half-maximum (HWHM), $\gamma(Q)$, of the Lorenztian, $\mathcal{L}(Q,\omega)$, which represents the broadened energy distribution that results from neutron−nucleus collisions and corresponds to the population statistics of one relaxation process, the QENS spectra were fitted using the following function,

$$\begin{aligned} S(Q,\omega) = {} & [EIS\,F(Q)\delta(\omega) \\ & + (1 - EIS\,F(Q))\mathcal{L}(Q,\omega)] \circledast R(Q,\omega), \end{aligned} \tag{10}$$

where $R(Q,\omega)$ denotes the resolution function of the instrument and defines the observation time of the spectrometer. The symbol $\mathcal{L}(Q,\omega)$ stands for a Lorentzian function,

$$\mathcal{L}(Q,\omega) = \frac{1}{\pi}\frac{\gamma(Q)}{\gamma(Q)^2 + \omega^2}. \tag{11}$$

The observed QENS spectra essentially arise from the translational diffusion of the molecules and we use here the well-established jump diffusion model (JDM) [1] to describe the experimental data, with the Chudley-Elliot relaxation rate

$$\gamma_{\mathrm{CE}}(Q) = \frac{D_t Q^2}{1 + D_t Q^2 \tau_0} \tag{12}$$

where D_t is the translation diffusion coefficient and τ_0 the residence time, i.e. the time between the discrete jumps of the hydrogen atoms.

The fit with a single Lorentzian, $\mathcal{L}(Q,\omega)$ corresponds to choosing the relaxation function in the generic form (5) of the intermediate scattering function to be an exponentially decaying function for $t > 0$,

$$\phi^{(+)}_{\mathrm{JDM}}(Q,t) = \exp(-\gamma(Q)|t|), \tag{13}$$

which is symmetrized by choosing the absolute value of t as argument.

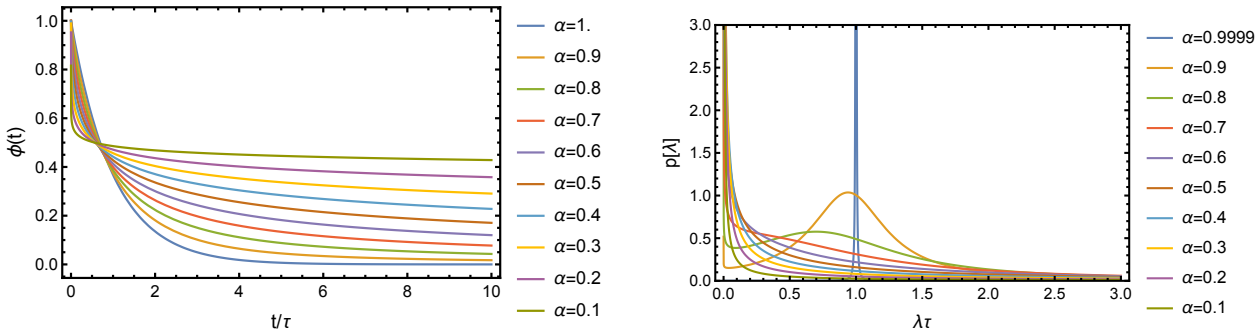

Figure 1. Left panel: Model relaxation function, $E_\alpha(-(|t|/\tau)^\alpha)$, for $0 < \alpha \leq 1$. **Right panel:** The corresponding relaxation rate spectra defined by Eq. (18).

3.2 "Minimalistic" multi-scale relaxation model

The QENS data were also analyzed in the time domain using a "minimalistic" multi-timescale relaxation model (MRM) [12, 13, 14]. The intermediate scattering function required for such analysis was obtained by Fast Fourier transforming the experimental QENS spectra. In the fitting procedure the generic form of the intermediate scatting function, Eq. 8, is assumed to have a (symmetrized) relaxation function of the form of a stretched Mittag-Leffler (ML) function [12, 13, 14] (the Q-dependence is omitted here),

$$\phi^{(+)}_{\rm ML}(t) \equiv E_\alpha(-(|t|/\tau)^\alpha) \quad (0 < \alpha \leq 1, \tau > 0), \quad (14)$$

which can be considered a generalization of the exponential function and admit $EISF(Q) > 0$. We note that,

$$E_\alpha(z) = \sum_{k=0}^{\infty} \frac{z^k}{\Gamma(1+k\alpha)} \quad (15)$$

is an entire function in the complex plane [21], where $\Gamma(z)$ is the generalized factorial [22], and that the exponential function is retrieved in the special case $\alpha = 1$. Here α sets the form of the relaxation function and τ its time scale. The left panel of Fig. 1 shows the model relaxation function for various values of α. For $0 < \alpha < 1$ the stretched ML function takes a scale-invariant power law form,

$$\phi^{(+)}_{\rm ML}(t) \overset{t\gg\tau}{\sim} \frac{(t/\tau)^{-\alpha}}{\Gamma(1-\alpha)}, \quad (16)$$

and since $\lim_{z\to 0}\Gamma(z) = \infty$, this long time tail will vanish for $\alpha \to 1$, i.e for exponential relaxation. The Q-dependent parameters in the above model are thus α, determining the form of the relaxation function, τ, setting the time scale, and the EISF [23].

Important for the following discussions is that the stretched ML function can be written as a continuous superposition of exponentially decaying functions,

$$\phi^{(+)}_{\rm ML}(t) = \int_0^\infty d\lambda\, p_{\alpha,\tau}(\lambda) e^{-\lambda t} \qquad (t \geq 0) \quad (17)$$

where the relaxation rate spectrum, $p_{\alpha,\tau}(\lambda)$, has the form [24],

$$p_{\alpha,\tau}(\lambda) = \frac{\sin(\pi\alpha)}{\pi\lambda\left((\lambda\tau)^{-\alpha} + (\lambda\tau)^{\alpha} + 2\cos(\pi\alpha)\right)}. \quad (18)$$

The above relaxation rate spectrum fulfills the conditions of a probability distribution, which are positivity, $p_{\alpha,\tau}(\lambda) \geq 0$, and normalization, $\int_{-\infty}^{+\infty} d\lambda\, p_{\alpha,\tau}(\lambda) = 1$. The right panel of Fig. 1 shows the relaxation rate spectrum for different values of α on a dimensionless scale, where $\tau = 1$. We note here that all moments $\langle\lambda^k\rangle \equiv \int_{-\infty}^{+\infty} d\lambda\, \lambda^k p_{\alpha,\tau}(\lambda)$ diverge for $k \geq 1$, which follows from the fact that, according to Eq. (14), $\langle\lambda^k\rangle = \partial_t^k \phi^{(+)}_{\rm ML}(t)\big|_{t=0}$, and that $\phi^{(+)}_{\rm ML}(t)$ is not differentiable at $t = 0$. The median, $\lambda_{1/2}$, and which is defined through $\int_0^{\lambda_{1/2}} d\lambda\, p_{\alpha,\tau}(\lambda) = 1/2$, has, however, the particularly simple form,

$$\lambda_{1/2} = 1/\tau, \quad (19)$$

which will be used in the following.

4 Experimental and computational methods

4.1 Experimental details and data reduction

Data on bulk-water were collected using IRIS, a cold neutron indirect backscattering spectrometer installed at the ISIS Spallation Neutron and Muon source. The spectrometer provides an intrinsic energy resolution of 17.5 μeV (FWHM), corresponding to an upper experimental observation of $\approx$ 200 ps for those scattered neutrons energy analysed at $\lambda = 6.3$Å [8]. The bulk-water sample was mounted in a cylindrical sample holder and measurements were conducted at 300K.

The measured dynamic structure factor is inevitably resolution broadened, which can be mathematically expressed through the convolution integral

$$S_m(Q,\omega) = \int_{-\infty}^{+\infty} d\omega'\, R(Q,\omega-\omega') S(Q,\omega), \quad (20)$$

where the index "m" stands for "measured". A vanadium standard, that can be considered a completely elastic and isotropic material, is used to define the intrinsic resolution function of the spectrometer, $R(Q,\omega)$, and calibrate the measured data. Such intrinsic broadening is accounted for using the reduction and analysis program Mantid [25]. After calibration and background subtraction, using data

collected from an empty sample container, the measured QENS spectra were transformed into the dynamic structure factor, $S(Q,\omega)$, and the spectrum grouped to obtain 9 constant scattering vectors in the range $0.55\text{Å}^{-1} \leq Q \leq 1.85\text{Å}^{-1}$.

4.2 MD simulation and analysis

A cubic box of 1728 water molecules, with a side length of $3.72nm$, was simulated at $300K$ using the SPCE force field [26] and applying periodic boundary conditions. Coulomb interactions in presence of periodic boundary conditions were treated by the particle-particle-particle-mesh (PPPM) method [27] and the Lennard-Jones part of the potential was cut at $1.4\,nm$. Prior to the production run, the system was energy minimized and subsequently equilibrated. The production run was performed for 1 ns, with a time step of 1 fs and the Berendsen thermostat [28] was used to keep the system at the desired temperature of $300K$. During the production run, the positions and velocities of the atoms were saved every $0.01ps$ and the SHAKE algorithm [29] was used to constrain the interatomic distances within the water molecules. The resulting MD trajectories were analysed using the nMoldyn software package [17, 18, 19, 20] which allowed direct comparison between the simulation results and the experimental data. Note that for this project some of the nMoldyn algorithms were rewritten in Python3 [30], and the physical quantities computed using Computerome [31].

5 Results and Discussion

5.1 Data analysis of the QENS spectra

The measured QENS spectra were analyzed

1. in the frequency domain, using the jump diffusion model Eq. (10), and
2. in the time domain, using the multiscale relaxation function (14) for the symmetrized relaxation function with the generic form (5) of the intermediate scattering function.

The details will be described separately in the following.

5.1.1 Data analysis with the jump diffusion model

The measured QENS spectra were first analysed using Eq. (10) and the Mantid software package [25]. Here a single Lorentzian relaxation is assumed and fast vibrational motions accounted for by adding a linear background term. As a result only a few priors were needed to analyse the data. The result of the fit and obtained parameters, are shown in Figs. 2a and 2b. The translational diffusion coefficient, obtained by fitting $\gamma(Q)$ using Eq. 12, was found to be $D_t = 2.38 \cdot 10^{-9} m^2/s$ and the residence time $\tau_0 = 0.61ps$, corresponding to a jump length of about 1 Å. These values are in agreement with the literature [4, 6]. The quality of the fit can be further verified by inspecting Fig. 3.

5.1.2 Data analysis with the multi-scale relaxation model

Here the QENS spectra are analyzed in the time domain, using the generic form given by Eq. (8) of the intermediate scattering function with the model relaxation function described by Eq. ((14). For the analysis three steps are performed. For more details we refer the reader to the original work describing the model [13]:

1. **Symmetrization the QENS spectra.** Based on the detailed balance relation, Eq (4), the QENS spectra are symmetrized with respect to ω,

$$S^{(+)}(Q,\omega) = \frac{e^{-\beta\hbar\omega/2} S(Q,\omega)}{\int_{-\infty}^{+\infty} d\omega\, e^{-\beta\hbar\omega/2} S(Q,\omega)} \qquad (21)$$

   which guarantees that $\int_{-\infty}^{+\infty} d\omega\, S^{(+)}(Q,\omega) = F^{(+)}(Q,0) = 1$. By defining and using $S^{(+)}(Q,\omega)$ we make sure that our spectra are symmetric and fulfill the detail balance relation, making it possible to easily Fourier transform the spectra and describe it using semi-classical models [13].

2. **Compute and deconvolve the intermediate scattering function.** Assuming that the resolution function, Eq. 20, is symmetric in ω, the "measured" intermediate scattering function is computed using a discrete approximation of the inverse Fourier transform $F_m^{(+)}(Q,t) = \int_{-\infty}^{+\infty} d\omega\, e^{i\omega t} S_m^{(+)}(Q,\omega)$. By writing $F_m^{(+)}(Q,t) = R(Q,t) S^{(+)}(Q,t)$ according to the convolution theorem of the Fourier transform, we obtain,

$$F^{(+)}(Q,t) = F_m^{(+)}(Q,t)/R(Q,t) \quad \text{for} \quad |t| < t_c. \qquad (22)$$

   The cutoff time is determined by the resolution ΔE (FWHM) of the instrument, writing $t_c = \hbar/2\Delta E$. An explicit illustration can be found in Ref. [23].

3. **Parameter fit.** Once the experimental data was reduced following the steps described above, the deconvolved $F^{(+)}(Q,t)$ was fitted using Eq. (8) using the IMinuit package [32]. This approach uses a least-square fitting routine to find the set of parameters which minimize the χ^2-value [32].

The result of fitting $F^{(+)}(Q,t)$ with Eq. (14) is shown at selected Q-value Fig. 2c. It can be observed that the model follows the experimental data quite well. From the fit parameters, shown in Fig. 2d, we note that the evolution of $\alpha(Q)$ accounts for a certain heterogeneity of the local environment of the diffusing water molecules, which becomes visible on increasingly larger spatial scales where $\alpha(Q) \approx 0.9$. Besides, the fact that local motions are faster than more delocalized ones is clearly reflected by the decay of the relaxation time scale $\tau(Q)$ with Q.

5.1.3 Comparing the results obtained in frequency and time domain

We start the comparison between the results of the QENS data analyses with the two models by resuming that the

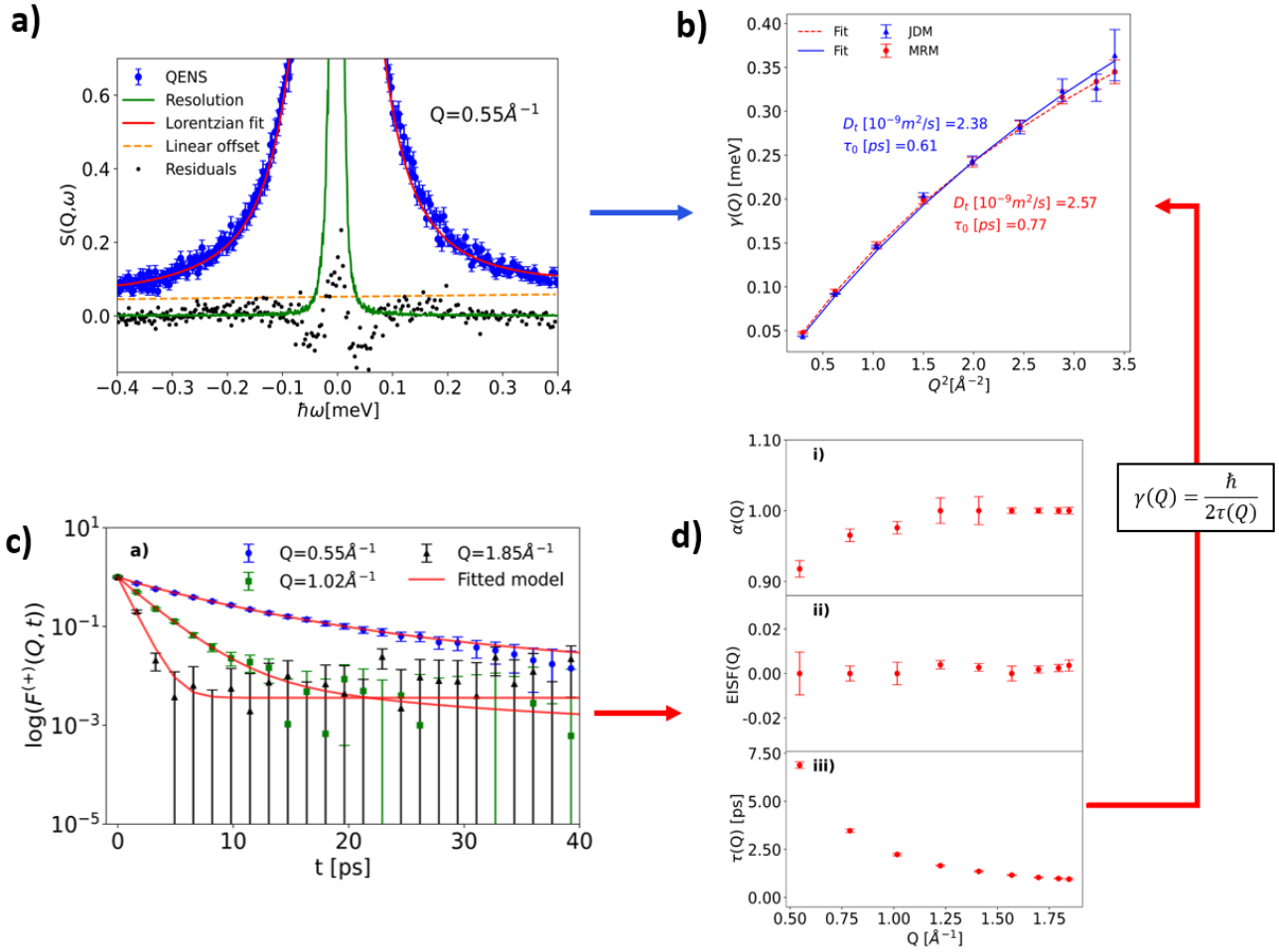

Figure 2. Overview of the data analysis performed on the QENS spectra for bulk-water at $300K$. a) The jump diffusion model (JDM) fit of the dynamic structure factor, $S(Q,\omega)$, according to Eq. 10. The residuals between the Lorentzian fit and the QENS spectrum are also plotted along with the resolution and the linear background. b) The half width at half maximum (HWHM) $\gamma(Q)_{JDM}$ values extracted from each JDM fit as a function of Q^2, compared to the HWHM $\gamma(Q)_{MRM}$ determined from the $\tau(Q)$ parameter of the multi-scale relaxation model (MRM). Both sets of HWHM data are fitted using, Eq. 12, where the fit results are presented above/below the fit in a corresponding color. c) MRM fit of the symmetrized, normalized, and deconvolved intermediate scattering function, $F^{(+)}(Q,t)$, according to Eq. 8. d) Water dynamics parameters of the QENS spectra as a function of Q obtained from the MRM model fit of $F^{(+)}(Q,t)$: i) $\alpha(Q)$, ii) the $EIS\,F(Q)$, and iii) $\tau(Q)$. The lack of Q-dependence and zero value for the $EIS\,F(Q)$ reflects that, as expected, the water molecules are not spatially constrained.

JDM describes the relaxation of the intermediate scattering function with a single exponential function, Eq. (13), whereas the MRM describes the relaxation with a stretched Mittag-Leffler function, Eq. (14). Trivially $\gamma(Q) = 1/\tau(Q)$ in the limit $\alpha \to 1$, where $\phi^{(+)}_{\mathrm{ML}}(t) = \phi^{(+)}_{\mathrm{JDM}}(t)$, but the interesting question is how $1/\tau(Q)$ compares to $\gamma(Q)$ for $\alpha < 1$. The answer is given in Fig. 2b, which shows that $\gamma(Q) \approx 1/\tau(Q)$ over the whole Q-range and that thus for both models (JDM and MRM) yield similar values are obtained for the parameters D_t and τ_0. This is an important result since it shows that the MRM can be considered as a refined form of the JDM, in the sense that the Chudely-Elliot model is a physical model for the median of the MRM,

$$\lambda_{1/2}(Q) \approx \gamma_{\mathrm{CE}}(Q). \tag{23}$$

This also further confirms that the multi-scale relaxation model is able to fully capture the complex and heterogeneous relaxation processes of the intermediate scattering function without prior assumptions and a minimal number of fit parameters.

5.2 Reproducing the experimental spectra by MD simulations

To verify that the MD simulation reproduces the QENS data, we compare the results graphically for three different Q-values in Fig. 4. Here the QENS data were transformed into $F^{(+)}(Q,t)$ following steps 1-2 described in Section 5.1, while the produced trajectories of the MD simulations were converted into the intermediate scattering function of the form $F(Q,t)$, using rewritten algorithms from nMoldyn [30]. Note that the coherent part of $F(Q,t)$ is omitted for the MD simulations, since we assume that only the incoherent contribution is probed in the experiment.

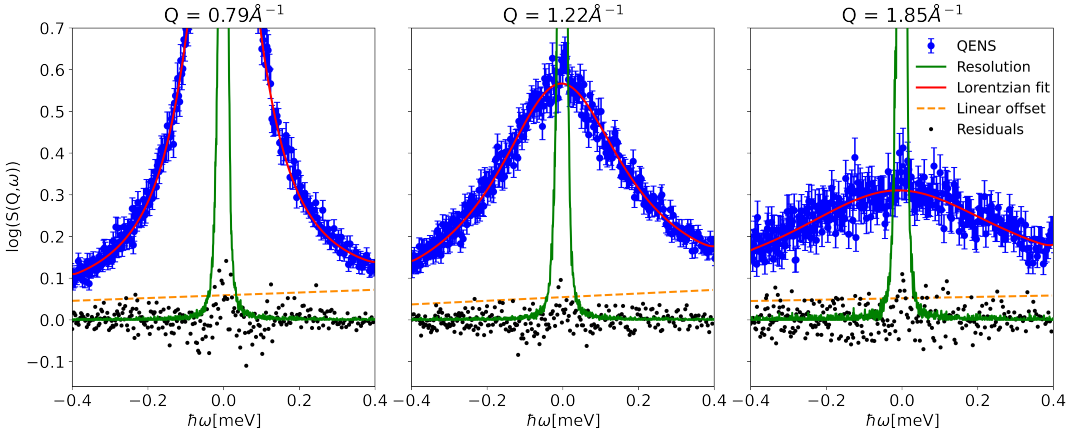

Figure 3. Zoom of the QENS experimental spectra for bulk-water at 300 K fitted using the jump diffusion model (JDM), according to Eq. 10 at three different Q-values. The residuals between the Lorentzian fit and the QENS spectrum are also plotted along with the resolution and the linear background.

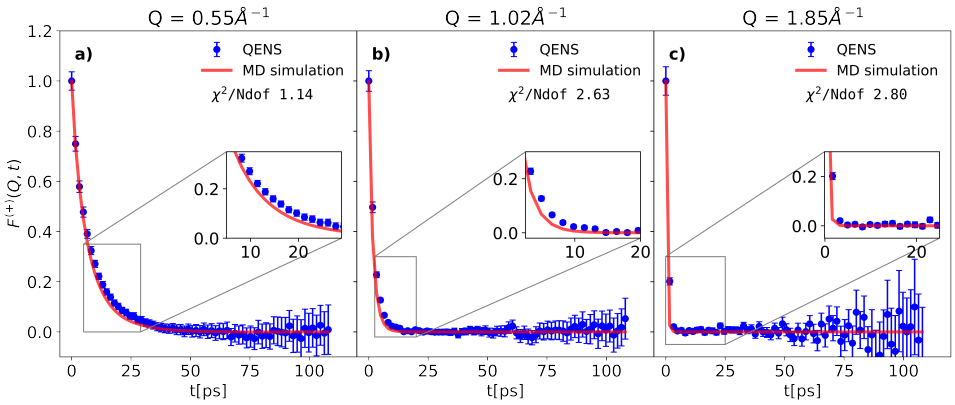

Figure 4. The symmetrized, normalised and deconvolved intermediate scattering function, $F^{(+)}(Q,t)$, for the QENS data and the MD simulation of bulk-water at $300K$, at three different Q-values.

Looking at Fig. 4, we observe that the MD simulation follows the QENS data at longer times. The large variation of $F^{(+)}(Q,t)$ with increasing computation time was previously noted in experimental QENS data [33] and is most likely related to the numerical Fourier transformation. Furthermore, considering that the dynamics of the system is hidden in the decay of $F^{(+)}(Q,t)$, we quantify the difference between the QENS data and MD simulation for all Q-values by the printed reduced χ^2-value. Here we observe that for higher Q-values the simulations do not reproduce the data equally well.

5.3 Reproducing the modelled spectra by MD simulations

Knowing that the MD simulation is comparable with the QENS data up to a certain point in time and space, we now evaluate the MD simulation output against the modelling approaches used to analyse the measured QENS data.

Using the MRM to inspect the MD results is straightforwardly done by fitting the simulated $F(Q,t)$ to Eq. 8. To consider the JDM, a free single exponential function is used to describe the diffusive motion. The results are depicted in Fig. 5a, where the two fitted models are plotted against the experimental data for two Q-values. We observe that the fitted curves follow the data in $F^{(+)}(Q,t)$ well. However, by analysing Fig. 5b, where the fitted models $F(Q,t)_{fit}$ are transformed into $S(Q,\omega)_{fit}$ and compared with the measured spectra, both models capture the measured QENS spectra particularly well for low Q-values only. This result can be better understood by analysing the evolution of $\gamma(Q)$, as a function of Q^2 obtained from the two models fits and depicted in Fig. 5d. We observe that for $Q > 1\text{Å}^{-1}$ the QENS data show asymptotic behavior, characteristic of jump diffusion of the atoms, while the MD simulations shows a linear growth indicating free diffusion with $D_t^{MD} \approx 3 \cdot 10^{-9} \frac{m^2}{s}$. As previously reported [6, 34], classic MD simulations have difficulties capturing the quantum effects of jump diffusion, making it plausible that the MD simulations continue probing free diffusion. This is somehow expected since the semi-classical approx-

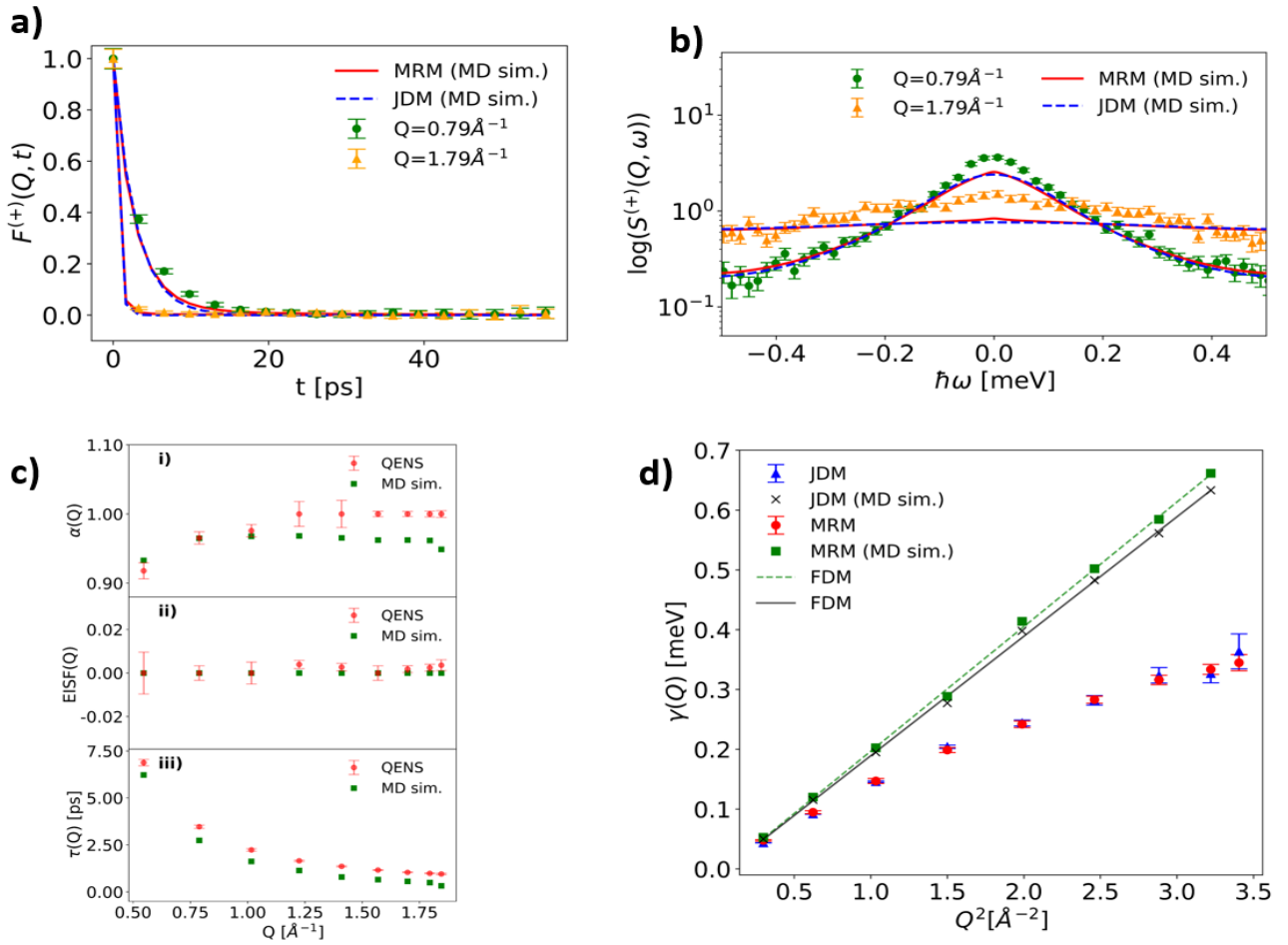

Figure 5. Overview of the data analysis performed on the MD simulation of bulk-water at 300K. a) The symmetrized, normalized, and deconvolved intermediate scattering function, $F^{(+)}(Q,t)$, of the QENS data for bulk-water at 300K plotted together with the jump diffusion model (JDM) fit and multi-scale relaxation model (MRM) fit of the MD simulation, according to a single exponential function and Eq. 8. b) The fitted models transformed into the symmetrized, normalized and convolved dynamic structure factor, $S^{(+)}(Q,\omega)$, plotted alongside the QENS spectra of bulk-water at 300K for comparison. c) Water dynamics parameters for the QENS data and MD simulation as a function of Q obtained from the multi-scale relaxation model fit of $F^{(+)}(Q,t)$: i) $\alpha(Q)$, ii) the $EISF(Q)$, and iii) $\tau(Q)$. The lack of Q-dependence and zero value for the $EISF(Q)$ reflects that, as expected, the water molecules are not spatially constrained. d) Extracted half width at half maximum (HWHM) $\gamma(Q)_{JDM(MD)}$ for each JDM fit of the QENS spectra and MD simulation as a function of Q^2, compared to the HWHM $\gamma(Q)_{MRM(MD)}$ determined from the $\tau(Q)$ parameter of the MRM fit of the QENS spectra and MD simulation. Both HWHM for the MD simulation are fitted using the free diffusion model (FDM), $\gamma(Q) = D_t Q^2 + const.$ resulting in $D_t^{JDM(MD)} = 3.04 \cdot 10^{-9} \frac{m^2}{s}$ and $D_t^{MRM(MD)} = 3.17 \cdot 10^{-9} \frac{m^2}{s}$. Both show minimal offset. Note that the HWHM for the last Q-value is omitted for the MD simulation, due to its larger size.

imation of the detailed balance relation, used to make the classical time correlation function equal to the quantum time correlation function, is only valid to the first order of $\hbar$ meaning that for high Q-values the approximation breaks down.

Now we turn to the evolution of the parameters of the MRM found by the fit of the MD simulation as a function of Q presented in Fig. 5c along with the fit parameters found for the QENS measured data. The following can be observed. (i) The value for the $\alpha(Q)$ parameter obtained by the two approaches agrees until $Q \approx 1.2\text{Å}^{-1}$, where it starts to diverge. This indicates that a slightly different diffusive motion of the hydrogen atoms is probed, where the MD simulation shows diffusion within a rougher harmonic potential, as the plateau value of $\alpha \approx 0.95$ suggests. (ii) $\tau(Q)$ shows the same Q-dependence with a 10% difference in magnitude, confirming that the MD simulation probes a faster diffusion.

6 Conclusions

Here, molecular dynamics (MD) simulations at 300K have been computed for bulk-water and compared to the measured quasi-elastic neutron scattering (QENS) spectra of the same system. The intermediate scattering function $F(Q,t)$ for the MD simulations, computed using updated nMoldyn algorithms, could be related to the measured QENS spectra either in terms of $F(Q,t)$ or its Fourier transform; known as the dynamic structure factor $S(Q,\omega)$. The comparison was done graphically, with supporting χ^2-values, along with analysis using both the jump diffusion

model (JDM), consisting of fitting the measured spectra with a sum of Lorentzians, and a newly introduced "minimalistic" multi-scale relaxation model (MRM), which describes the the multi-scale relaxation of the hydrogen atoms of the measured spectra. The juxtaposition of the QENS data and the MD simulation for bulk-water showed that the MD simulation describes well the translational dynamics of the water relaxation. However, further investigation revealed that in reality the MD simulation cannot completely capture the discrete jumps occurring at more localized length scales where quantum effects becomes significant.

More importantly, by revisiting the modeling of QENS from bulk water, we show that the MRM, a new "minimalistic" energy landscape-based method for QENS analysis, can be used to accurately describe the data at all length scales. This is confirmed by comparing the Chudley-Elliot relaxation time and the relaxation time scale $\tau(Q)$ obtained from MRM, defining the *median relaxation rate* through $\lambda_{1/2}(Q) = 1/\tau(Q)$, and showing that these values follow on the same master curve.

References

[1] R.J. Elliott, C.T. Chudley, Proceedings of the Phys Society **77**, 353 (1961)
[2] P. Schofield, Phys Rev Letters **4**, 239 (1960)
[3] L. Van Hove, Phys Rev **95**, 249 (1954)
[4] J. Teixeira, Phys Rev. A, General Phys **31**, 913 (1985)
[5] H. Frauenfelder, P.W. Fenimore, R.D. Young, Proceedings of the National Academy of Sciences **111**, 12764 (2014)
[6] J. Qvist, et al., J Chem Phys **134**, 144508 (2011)
[7] H.N. Bordallo, et al., J Phys Chem C **112**, 13982 (2008)
[8] M.C. Berg, et al., ACS Applied Materials & Interfaces **10**, 9904 (2018)
[9] M.R. Harpham, et al., J Chem Phys **121**, 7855 (2004)
[10] R. Ignazzi, et al., J Phys Chem C **121**, 23582 (2017)
[11] T. Yamada, H. Seto, Front Chem. **8**, 8 (2020)
[12] G. Kneller, Proceedings of the National Academy of Sciences **115**, 9450 (2018)
[13] M. Saouessi, J. Peters, G.R. Kneller, J Chem Phys **150**, 161104 (2019)
[14] M. Saouessi, J. Peters, G.R. Kneller, J Chem Phys **151**, 125103 (2019)
[15] M.H. Petersen, et al., J Phys Chem C **125**, 15085 (2021)
[16] M. Childers, V. Daggett, J Phys Chem B **122**, 6673 (2018)
[17] G. Kneller, V. Keiner, M. Kneller, M. Schiller, Comp Phys Com **91**, 191 (1995)
[18] T. Róg, K. Murzyn, K. Hinsen, G. Kneller, J Comp Chem **24**, 657 (2003)
[19] V. Calandrini, E. Pellegrini, K. Hinsen, G. Kneller, École thématique de la Société Française de la Neutronique **12**, 201 (2011)
[20] K. Hinsen, E. Pellegrini, S. Stachura, G. Kneller, J Comp Chem **33**, 2043 (2012)
[21] R. Gorenflo, A.A. Kilbas, F. Mainardi, S.V. Rogosin, eds., *Mittag-Leffler Functions, Related Topics and Applications*, Springer Monographs in Mathematics (Springer, 2014)
[22] F.W.J. Olver, D.W. Lozier, R.F. Boisvert, *NIST handbook of mathematical functions hardback and CD-ROM* (Cambridge Univ Pr, 2010)
[23] A.N. Hassani, L. Haris, M. Appel, T. Seydel, A.M. Stadler, G.R. Kneller, J Chem Phys **156**, 025102 (2022)
[24] G.R. Kneller, Phys Chem Chem Phys **7**, 2641 (2005)
[25] O. Arnold, et al., Nuclear Instruments and Methods in Phys Research Section A: Accelerators, Spectrometers, Detectors and Associated Equipment **764**, 156 (2014)
[26] H.J.C. Berendsen, et al., J Phys Chem **91**, 6269 (1987)
[27] M.P. Allen, D.J. Tildesley, *Computer Simulation of Liquids* (Oxford, 2017)
[28] H.J.C. Berendsen, J.P.M. Postma, W.F. van Gunsteren, A. DiNola, J.R. Haak, J Chem Phys **81**, 3684 (1984)
[29] J.P. Ryckaert, G. Ciccotti, H.J. Berendsen, J Comp Phys **23**, 327 (1977)
[30] M.H. Petersen, *Overview of the used code*, Published at https://github.com/ in a private repository and access can be obtained by writing to martinhp27@gmail.com (2022)
[31] *Computerome: The danish national supercomputer for life sciences*, https://www.computerome.dk/display/C2W/Computerome+2.0+Wiki
[32] H. Dembinski, P. Ongmongkolkul, C. Deil et al., Zenodo, doi **10** (2020)
[33] M.T.F. Telling, et al., Soft Matter **7**, 6934 (2011)
[34] T.O. Farmer, et al., J Phys Chem Letters **11**, 7469 (2020)